Impaired fatty acid import or catabolism in macrophages restricts intracellular growth of *Mycobacterium tuberculosis*

Nelson V. Simwela[1], Eleni Jaecklein [2], Christopher M. Sassetti[2], David G. Russell[1]*

1. Department of Microbiology and Immunology, College of Veterinary Medicine, Cornell University, Ithaca, New York, USA
2. Department of Microbiology, UMass Chan Medical School, Worcester, Massachusetts, USA

*Correspondence: dgr8@cornell.edu

Abstract

Mycobacterium tuberculosis (*Mtb*) infection of macrophages reprograms cellular metabolism to promote lipid retention. While it is clearly known that intracellular *Mtb* utilize host derived fatty acids and cholesterol to fuel the majority of its metabolic demands, the role of macrophage lipid catabolism on the bacteria's ability to access the intracellular lipid pool remains undefined. We utilized a CRISPR genetic knockdown approach to assess the impact of sequential steps in fatty acid metabolism on the growth of intracellular *Mtb*. Our analyzes demonstrate that knockdown of lipid import, sequestration and metabolism genes collectively impair the intracellular growth of *Mtb* in macrophages. We further demonstrate that modulating fatty acid homeostasis in macrophages impairs *Mtb* replication through diverse pathways like enhancing production of pro-inflammatory cytokines, autophagy, restricting the bacteria access to nutrients and increasing oxidative stress. We also show that impaired macrophage lipid droplet biogenesis is restrictive to intracellular *Mtb* replication, but increased induction of the same by blockade of downstream fatty acid oxidation fails to rescue *Mtb* growth. Our work expands our understanding of how host fatty acid homeostasis impacts *Mtb* growth in the macrophage.

Significance

Mycobacterium tuberculosis (*Mtb*) primarily infects macrophages in the lungs. In infected macrophages, *Mtb* uses host lipids as key carbon sources to maintain infection and survive. In this work, we used a CRISPR-Cas9 gene knockout system in murine macrophages to examine the role of host fatty acid metabolism on the intracellular growth of *Mtb*. Our work shows that macrophages which cannot either import, store or catabolize fatty acids restrict *Mtb* growth by both common and divergent anti-microbial mechanisms, including increased glycolysis, increased production of reactive oxygen species, production of pro-inflammatory cytokines, enhanced autophagy and nutrient limitation. Our findings demonstrate that manipulating lipid metabolism in macrophages controls *Mtb* through multiple other mechanisms, beyond limiting the bacteria's access to nutrients.

88 **Introduction**

89 *Mycobacterium tuberculosis* (*Mtb*), the causative agent of tuberculosis (TB), has caused disease
90 and death in humans for centuries (1). *Mtb* primarily infects macrophages in the lung (2, 3)
91 wherein the bacterium relies on host derived fatty acids and cholesterol for synthesis of its lipid
92 rich cell wall, and to produce energy and virulence factors (4-10). Within the lung
93 microenvironment, resident alveolar macrophages preferentially oxidize fatty acids and are more
94 permissive to *Mtb* growth while recruited interstitial macrophages are more glycolytic and
95 restrictive of *Mtb* replication (11-13). Globally, *Mtb* infection modifies macrophage metabolism
96 in a manner that enhances its survival. *Mtb* infected macrophages shift their mitochondrial
97 substrate preference to exogenous fatty acids which drives the formation of foamy macrophages
98 that are laden with cytosolic lipid droplets (4-6, 14, 15). Foamy macrophages are found in
99 abundance in the central and inner layers of granulomas, a common histopathological feature of
100 human TB (5, 16). Interference with key regulators of lipid homeostasis, such as the miR-33 and
101 the transcription factors peroxisome proliferator-activated receptor α (PPARα) and PPAR-γ
102 enhances macrophage control of *Mtb* (17-19). Moreover, compounds which modulate lipid
103 metabolism such as the anti-diabetic drug metformin and some cholesterol lowering drugs are
104 under investigation for host directed therapeutics (HDTs) against *Mtb* (20, 21). Although the
105 dependence of intracellular *Mtb* on host fatty acids and cholesterol is well documented (22), the
106 impact of specific aspects of macrophage lipid metabolism on the bacteria remains opaque. In
107 *Mtb* infected foamy macrophages, bacteria containing phagosomes are found in close apposition
108 to intracellular lipid droplets (4). It is believed that the bacterial induction of a foamy macrophage
109 phenotype in host cells results in a steady supply of lipids that addresses the bacteria's nutritional
110 requirements (4-7). In fact, intracellular *Mtb* has been shown to import fatty acids from host lipid
111 droplet derived triacylglycerols (7). However, other studies indicate that macrophage lipid droplet
112 formation in response to *Mtb* infection can lead to the induction of a protective, anti-microbial
113 response (23). *Mtb* appears unable to acquire host lipids when lipid droplets are induced by
114 stimulation with interferon gamma (IFN-γ) (23). Moreover, there is some evidence that lipid
115 droplets can be sites for the production of host protective pro-inflammatory eicosanoids (7, 23).
116 Lipid droplets can also act as innate immune hubs against intracellular bacterial pathogens by

117 clustering anti-bacterial proteins (24). Inhibition of macrophage fatty acid oxidation by knocking
118 out mitochondrial carnitine palmitoyl transferase 2 (CPT2) or using chemical inhibitors of CPT2
119 also restrict intracellular growth of *Mtb* (11, 25). These data demonstrate that modulation of the
120 different stages in lipid metabolism inside *Mtb* infected macrophages can result in conflicting
121 outcomes.
122
123 We carried out a candidate-based, CRISPR mediated knockdown of lipid import and metabolism
124 genes in macrophages to determine their roles in intracellular growth of *Mtb*. By targeting genes
125 involved in fatty acid import, sequestration, and metabolism in Hoxb8 derived conditionally
126 immortalized murine macrophages (26), we show that impairing lipid homeostasis in
127 macrophages at different steps in the process negatively impacts the growth of intracellular *Mtb*,
128 albeit to differing degrees. The impact on *Mtb* growth in the mutant macrophages was mediated
129 through different mechanisms despite some common anti-microbial effectors. *Mtb* infected
130 macrophages deficient in the import of long chain fatty acids increased production of pro-
131 inflammatory markers such as interleukin 1β (IL-1β). In contrast, ablation of lipid droplet
132 biogenesis and fatty acid oxidation increased production of reactive oxygen species and limited
133 the bacteria's access to nutrients. We also found that suppression of *Mtb* growth in macrophages
134 that are unable to produce lipid droplets could not be rescued by exogeneous addition of fatty
135 acids indicating that this is not purely nutritional restriction. Our data indicate that interference
136 of lipid metabolism in macrophages leads to suppression of *Mtb* growth via multiple routes.
137
138
139
140
141
142
143
144
145

146 **Results**

147 **Knockdown of fatty acid import and metabolism genes restricts *Mtb* growth in macrophages**

148 To apply a holistic approach to assessing the role(s) of fatty acid metabolism on the intracellular
149 growth of *Mtb*, we used a CRISPR genetic approach to knockout genes involved in lipid import
150 (CD36, FATP1), lipid droplet formation (PLIN2) and fatty acid oxidation (CPT1A, CPT2) in mouse
151 primary macrophages (Fig. 1A). Deletion of CD36 or CPT2 from mouse macrophages has been
152 shown to impair intracellular growth of *Mtb* (25, 27). But the role of specialized long chain fatty
153 acid transporters (FATP1-6) on *Mtb* growth in macrophages is uncharacterized. FATP1 and FATP4
154 are the most abundant fatty acid transporter isoforms in macrophages (28). PLIN2, or adipophilin,
155 is known to be required for lipid droplet formation (29, 30). Five isoforms of mammalian perilipins
156 (PLIN) are involved in lipid droplet biogenesis amongst which PLIN2 is the dominant isoform
157 expressed in macrophages (23). However, macrophages derived from PLIN2$^{-/-}$ mice show no
158 defects in production of lipid droplets nor do they impair intracellular growth of *Mtb* (23). We
159 targeted each of these genes with at least 2 sgRNAs in Hoxb8 Cas9^{+} conditionally immortalized
160 myeloid progenitors (26) to generate a panel of mutants that were deficient in the following
161 candidates of interest; FATP1$^{-/-}$, PLIN2$^{-/-}$, CD36$^{-/-}$, CPT1A$^{-/-}$ and CPT2$^{-/-}$. Each individual sgRNA
162 achieved >85% CRISPR-mediated deletion efficiency for all the 5 genes, as analyzed by the
163 Inference for CRISPR Edits (ICE) tool (31) (Table. S1). We verified the protein knockdown
164 phenotypes by flow cytometry and western blot analysis of differentiated macrophages derived
165 from the CRISPR deleted Hoxb8 myeloid precursors (Fig. S1).

166 To confirm certain knockdown phenotypes functionally, we checked lipid droplet
167 biogenesis in PLIN2$^{-/-}$ macrophages in comparison to macrophages transduced with a non-
168 targeting scramble sgRNA by confocal microscopy of BODIPY stained cells. Cells were cultured for
169 24 hours in the presence of exogenous oleate to enhance the formation of lipid droplets (32). We
170 observed a complete absence of lipid droplet formation in PLIN2$^{-/-}$ macrophages as compared to
171 controls (Fig. S2). This is contrary to previous observations in macrophages derived from PLIN2
172 knockout mice which were reported to have no defect in lipid droplet formation (23). We also
173 assessed the ability of CPT2$^{-/-}$ macrophages to oxidize fatty acids using the Agilent Seahorse XF
174 Palmitate Oxidation Stress Test. Scrambled sgRNA and CPT2$^{-/-}$ macrophages were cultured in

175 substrate limiting conditions and supplied with either bovine serum albumin (BSA) or BSA
176 conjugated palmitate. As shown in Fig. S2B, control macrophages were able to utilize and oxidize
177 palmitate in substrate limiting conditions indicated by a significant increase in oxygen
178 consumption rates (OCRs) in contrast to cells supplied with BSA alone. Addition of the CPT1A
179 inhibitor, etomoxir, inhibited the cell's ability to use palmitate in these conditions (Fig. S2B). CPT2
180 knockdown in CPT2$^{-/-}$ macrophages impaired the cell's ability to oxidize palmitate to a degree
181 comparable to etomoxir treatment as evidenced by baseline OCRs when compared to scrambled
182 sgRNA control (Fig. S2C).

183 We then assessed the different knockdown mutant macrophages in their ability to support
184 the intracellular growth of *Mtb*. We infected macrophages with *Mtb* Erdman at a multiplicity of
185 infection (MOI) of 0.4 and assessed intracellular bacterial growth rates by counting colony forming
186 units (CFUs) 5 days post infection. All the 5 mutant macrophages significantly impaired *Mtb*
187 growth rates when compared to scrambled sgRNA as assessed by CFUs counts on day 5 (Fig. 1C).
188 PLIN2$^{-/-}$, FATP1$^{-/-}$ and CPT2$^{-/-}$ macrophages displayed the strongest growth restriction phenotypes
189 while CD36$^{-/-}$macrophages had a moderate, but significant, impact on *Mtb* growth. We quantified
190 intracellular bacteria on day 0, 3 hours post infection (Fig. 1B), to ascertain that subsequent
191 differences on day 5 were not due to defects in initial phagocytosis. The moderate growth
192 restriction phenotypes of CD36$^{-/-}$ macrophages were consistent with previous findings which
193 reported similar impact on *Mtb* and *M. marinum* growth in macrophages derived from CD36$^{-/-}$
194 mice (27). Impaired growth of *Mtb* in CPT1A$^{-/-}$ and CPT2$^{-/-}$ macrophages is also consistent with
195 previous reports that genetic and chemical inhibition of fatty acid oxidation is detrimental to the
196 growth of *Mtb* within macrophages (11, 25).

197

198 ***Mtb* infected macrophages with impaired fatty acid import and metabolism display altered**
199 **mitochondrial metabolism and elevated glycolysis.**

200 Impairment of fatty acids metabolism by FATP1 knockout in macrophages rewires their substrate
201 bias from fatty acids to glucose (33). We reasoned that deletion of genes required for downstream
202 processing of lipids (Fig. 1A) could also reprogram macrophages and increase glycolysis which
203 could, in part, explain bacterial growth restriction. We analyzed the metabolic states of 3

204 knockout macrophages (FATP1$^{-/-}$, PLIN2$^{-/-}$ and CPT2$^{-/-}$) in uninfected and *Mtb* infected conditions
205 by monitoring oxygen consumption rates (OCR) and extracellular acidification rates (ECARs) using
206 the Agilent Mito and Glucose Stress Test kits. All 3 mutant uninfected macrophages displayed
207 reduced mitochondrial respiration as evidenced by lower basal and spare respiratory capacity
208 (SRC) when compared to scrambled sgRNA controls (Fig. S3A, 3SB). *Mtb* infection proportionally
209 reduced basal and SRC rates across all the mutant macrophages and scrambled controls (Fig. 2A,
210 2B) when compared to uninfected macrophages, which is consistent with previous findings (14).
211 PLIN2$^{-/-}$ macrophages displayed the most marked reduction in mitochondrial activity in both
212 uninfected and infected conditions, while FATP1$^{-/-}$ macrophages were the least affected (Fig. 2A,
213 Fig. S3A). As reported previously (33), uninfected FATP1$^{-/-}$ macrophages were more glycolytically
214 active with higher basal and spare glycolytic capacity (SGC) compared to scrambled controls (Fig.
215 S3D, S3E). Uninfected PLIN2$^{-/-}$ and CPT2$^{-/-}$ macrophages were also more glycolytically active, but
216 to a greater degree than FATP1$^{-/-}$ (Fig. S3D, S3E). *Mtb* infection increased the glycolytic capacity
217 of all the 3 mutant macrophages (Fig. 2C, 2D). Overall, PLIN2$^{-/-}$ macrophages exhibited the highest
218 glycolytic capacity (Fig. 2C, Fig. S3D). Our data indicates that impairment of fatty acid metabolism
219 at different steps significantly impacts mitochondrial respiration and reprograms cells towards
220 glycolysis. Increased glycolytic flux in macrophages has been linked to the control of intracellular
221 *Mtb* growth (34, 35). Metabolic realignment as a consequence of interference with lipid
222 homeostasis, which results in enhanced glycolysis may contribute to *Mtb* growth restriction in
223 these mutant macrophages.
224

225 **Knockdown of lipid import and metabolism genes in macrophages activates AMPK and**
226 **stabilizes HIF-1α**

227 *Mtb* infection is known to induce increased glycolysis or the "Warburg effect" in macrophages,
228 mouse lungs and human TB granulomas (34-36). Several studies have demonstrated that the
229 Warburg effect is mediated by the master transcription factor hypoxia-inducible factor-1 (HIF-1)
230 (37). During *Mtb* infection, HIF-1 is activated by production of reactive oxygen species (ROS), TCA
231 cycle intermediates and hypoxia in the cellular microenvironments as a consequence of altered
232 metabolic activities and increased immune cell functions (34-36, 38). We assessed HIF-1 stability

233 in the 3 mutant macrophage lineages (FATP1$^{-/-}$, PLIN2$^{-/-}$ and CPT2$^{-/-}$) by monitoring total HIF-1α
234 protein levels by western blot, having confirmed that they were all more glycolytically active than
235 the scrambled controls (Fig. 2, Fig. S3). Indeed, all the 3 mutant macrophages displayed
236 significantly higher amounts of total HIF-1α when compared to scrambled controls in uninfected
237 conditions and after *Mtb* infection for 48 hours (Fig. 3A, 3B). We also checked the phosphorylation
238 status of the adenosine monophosphate kinase (AMPK), a master regulator of cell energy
239 homeostasis (39), in the mutant macrophages since Seahorse flux analyses indicated that they
240 had impaired mitochondrial activities (Fig. 2, Fig. S3). Western blot analysis revealed that in both
241 *Mtb* infected and uninfected conditions, impaired fatty acid metabolism correlated with
242 moderate activation of AMPK as indicated by increased AMPK phosphorylation (Fig. 3C, 3D).
243 These data point to a metabolic reprogramming of cells through activation of HIF-1α and AMPK
244 to promote glycolysis. In energetically stressed cellular environments, activated AMPK promotes
245 catabolic processes such as autophagy to maintain nutrient supply and energy homeostasis (39).
246 Autophagy is also an innate immune defense mechanism against intracellular *Mtb* in
247 macrophages (40). We examined the levels of autophagic flux in the mutant macrophages by
248 monitoring LC3I to LC3II conversion by western blot and by qPCR analysis of selected autophagy
249 genes (*AMBRA1*, *ATG7*, *MAP1LC3B* and *ULK1)*. We observed a moderate increase in autophagic
250 flux by western blot in uninfected FATP1$^{-/-}$ and CPT2$^{-/-}$ macrophages, which was amplified upon
251 infection with *Mtb* (Fig. S4A, S4B). Our qPCR analysis revealed that the 4 autophagy genes were
252 upregulated in both *Mtb* infected and uninfected conditions in all the 3 mutants (Fig. S4C, S4D).
253 These data suggest that impaired fatty acid import and metabolism in macrophages could be
254 restricting *Mtb* growth by promoting autophagy. These data agree with previous observations
255 that inhibition of fatty acid oxidation enhances macrophage xenophagic activity whichleads to
256 improved control of *Mtb* (25).
257

258 **Exogenous oleate fails to rescue the *Mtb icl1*-deficient mutant in FATP1$^{-/-}$, PLIN2$^{-/-}$ and CPT2$^{-/-}$**
259 **macrophages**

260 The mycobacterial isocitrate lyase (*icl1*) acts as an isocitrate lyase in the glyoxylate shunt and as a
261 methyl-isocitrate lyase in the methyl-citrate cycle (MCC) (41, 42). *Mtb* uses the MCC to convert

262 propionyl CoA originating from the breakdown of cholesterol rings and β-oxidation of odd chain
263 fatty acids into succinate and pyruvate, which are eventually assimilated into the TCA cycle (43,
264 44). The buildup of propionyl CoA is toxic to *Mtb* and the bacteria relies on the MCC together with
265 the incorporation of propionyl CoA to methyl-branched lipids in the cell wall as an internal
266 detoxification system (43, 45). *Mtb* propionyl CoA toxicity is, in part, due to a cellular imbalance
267 between propionyl CoA and acetyl CoA as an accumulation of the former or paucity of the latter
268 results in the propionyl CoA mediated inhibition of pyruvate dehydrogenase (46). Consequently,
269 *Mtb icl1* deficient mutants (*Mtb ⊿icl1*) are unable to grow in media supplemented with
270 cholesterol or propionate, or intracellularly in macrophages (46). However, this growth inhibition
271 could be rescued both in culture and in macrophages by exogenous supply of acetate or even
272 chain fatty acids which can be oxidized to acetyl-CoA (46). We took advantage of this metabolic
273 knowledge to assess whether exogenous addition of the even chain fatty acid oleate can rescue
274 the intracellular growth of *Mtb ⊿icl1* mutants in our CRISPR knockdown macrophages. Scrambled
275 controls, FATP1$^{-/-}$, PLIN2$^{-/-}$ and CPT2$^{-/-}$ macrophages in normal macrophage media or media
276 supplemented with oleate were infected with an *Mtb ⊿icl1* strain expressing mCherry at MOI 5.
277 Bacterial growth measured by mCherry expression was recorded 5 days post infection. Consistent
278 with previous observations (46), the *Mtb ⊿icl1* mutant failed to replicate in both mutant and
279 scramble macrophages that were grown in normal macrophage media as evidenced by baseline
280 mCherry fluorescence (Fig. 4A). Oleate supplementation successfully rescued the *Mtb ⊿icl1*
281 mutant in scrambled control macrophages. However, the growth restriction of the *Mtb ⊿icl1*
282 strain could not be alleviated by exogenous addition of oleate to the mutant macrophages (FATP1^{-}
283 $^{/-}$, PLIN2$^{-/-}$ and CPT2$^{-/-}$) (Fig. 4A). These data suggest that impaired import (FATP1$^{-/-}$), sequestration
284 (PLIN2$^{-/-}$) or β-oxidation of fatty acids (CPT2$^{-/-}$) blocks *Mtb*'s ability to access and use cellular lipids.
285 Oleate supplementation in macrophages induces the formation of lipid droplets and we
286 were able to confirm the inability to produce lipid droplets in PLIN2$^{-/-}$ macrophages using this
287 approach (Fig. S2A). As an indirect measure to track the fate of supplemented oleate in the
288 mutant macrophages, we monitored lipid droplet biogenesis in FATP1$^{-/-}$ and CPT2$^{-/-}$ macrophages
289 to check if the inability to rescue the *Mtb ⊿icl1* impaired growth phenotypes in these mutant
290 macrophages could be possibly related to disruptions in lipid droplet biogenesis. Confocal analysis

291 of BODIPY stained cells upon oleate supplementation revealed that FATP1$^{-/-}$ macrophages also fail
292 to generate lipid droplets (Fig. 4B). In contrast, CPT2$^{-/-}$ macrophages produced more and larger
293 lipid droplets in comparison to scrambled controls (Fig.4B). These data suggest that the inhibition
294 of *Mtb* growth in these mutant macrophages is not merely through limitation of access to fatty
295 acid nutrients.
296
297 **Dual RNA sequencing to identify host and bacterial determinants of *Mtb* restriction in mutant**
298 **macrophage lineages.**
299 We performed RNA sequencing of both host and bacteria in *Mtb* infected mutant macrophages
300 as a preliminary step in identification of pathways restricting bacterial growth. We infected
301 scrambled controls, FATP1$^{-/-}$, PLIN2$^{-/-}$ and CPT2$^{-/-}$ macrophages with the *Mtb* smyc'::mCherry
302 strain for 4 days and processed the samples for dual RNA sequencing as previously described (47).
303 Principal component analysis (PCA) of host transcriptomes revealed a clustering of all the 3
304 mutant macrophages away from scrambled controls (Fig. 5A). Interestingly, there was a
305 separation in transcriptional responses between the 3 mutant macrophages as CPT2$^{-/-}$ and PLIN2^{-}
306 $^{/-}$ macrophages clustered closer together and more distant from FATP1$^{-/-}$ (Fig. 5A). Overall, using
307 an adjusted p-value < 0.05 and absolute log2 fold change > 1.2, we identified 900 genes which
308 were differentially expressed (DE) in PLIN2$^{-/-}$ macrophages (589 up, 311 down), 817 genes which
309 were DE in FATP1$^{-/-}$ macrophages (501 up, 315 down) and 189 genes which were DE in CPT2$^{-/-}$
310 (124 up, 65 down) (Table. S2, Fig.5B). Consistent with the PCA analysis, Venn diagram of the DE
311 genes (Fig.5B) indicated divergent responses in the 3 mutant macrophage populations. We
312 performed pathway enrichment analysis (48) of the DE genes to identify anti-microbial pathway
313 candidates in the 3 mutant macrophages. We found that defects in fatty acid uptake in FATP1$^{-/-}$
314 infected macrophages upregulated pro-inflammatory pathways involved in MAPK and ERK
315 signaling and production of inflammatory cytokines (IFN-γ, interleukin-6, Interleukin-1α, β) (Fig.
316 5D, Table. S3). The pro-inflammatory signatures of the FATP1$^{-/-}$ macrophages are consistent with
317 previous observations that demonstrated that a deficiency in FATP1 exacerbated macrophage
318 activation *in vitro* and *in vivo* (33). FATP1 is a solute carrier family member (SLC27A1) and *Mtb*
319 infected FATP1$^{-/-}$ macrophages showed reduced expression of other solute carrier transporters

320 (SLC) such as FATP4 (SLC27A4), GLUT1 (SLC2A1) and 8 SLC amino acid transporters (Fig. S7A, S7B,
321 Table. S2). Interestingly, *Mtb* infected FATP1$^{-/-}$ macrophage transcriptomes exhibited upregulation
322 of macrophage scavenger receptors (MSR1) and the ATP binding cassette transporter ABCC1 (Fig.
323 S7A), both of which can independently transport fatty acids into cells (49, 50).

324 Meanwhile, inability generate lipid droplets in *Mtb* infected PLIN2$^{-/-}$ macrophages led to
325 upregulation in pathways involved in ribosomal biology, MHC class 1 antigen presentation,
326 canonical glycolysis, ATP metabolic processes and type 1 interferon responses (Fig. 5C, Table. S3).
327 In the downregulated PLIN2$^{-/-}$ DE gene set, enriched pathways included those involved in
328 production of pro-inflammatory cytokines; interleukin-6 and 8, IFN-γ and interleukin-1 (Fig. S5A,
329 Table. S3). Oxidative phosphorylation and processes involved in the respiratory chain electron
330 transport were also significantly enriched in PLIN2$^{-/-}$ downregulated genes. This suggests that *Mtb*
331 infected PLIN2$^{-/-}$ macrophages increase glycolytic flux and decrease mitochondrial activities,
332 which is consistent with our metabolic flux analysis data (Fig.2). Unlike FATP1$^{-/-}$ macrophages,
333 PLIN2$^{-/-}$ macrophages are, however, broadly anti-inflammatory as most pro-inflammatory genes
334 were downregulated upon *Mtb* infection.

335 Further downstream in the lipid processing steps, inhibition of fatty acid oxidation in CPT2^{-}
336 $^{/-}$ macrophages upregulated pathways involved in MHC class 1 antigen presentation, response to
337 IFN-γ and interleukin-1 and T-cell mediated immunity (Fig. S6, Table. S3). There was a limited
338 overlap in enriched pathways in the upregulated genes between *Mtb* infected CPT2$^{-/-}$ and FATP1^{-}
339 $^{/-}$ macrophages such as those involved in the cellular responses to interleukin-1 and IFN-γ.
340 However, many pathways over-represented in CPT2$^{-/-}$ macrophages were common to PLIN2$^{-/-}$
341 macrophages (Fig. 5C, Fig. S6, Table. S3). Similarly, both *Mtb*-infected PLIN2$^{-/-}$ *and* CPT2$^{-/-}$
342 macrophages were downregulated in expression of genes involved in oxidative phosphorylation
343 (Table. S3). We confirmed expression levels of key genes by qPCR analysis of IL-1β and the type 1
344 interferon (IFN-β) response during the early time points of infection. Indeed, 4 hours post
345 infection, IL-1β and IFN-β were both upregulated in FATP1$^{-/-}$ macrophages as compared to
346 scrambled controls consistent with their pro-inflammatory phenotype (Fig. S8A, S8B). On the
347 contrary, PLIN2$^{-/-}$ macrophages downregulated IL-1β (Fig. S8B). These data indicate that

348 macrophages respond quite divergently to the deletion of the different steps in fatty acid uptake,
349 which implies that the intracellular pressures to which *Mtb* is exposed may also differ.
350
351 **Oxidative stress and nutrient limitation are major stresses experienced by *Mtb* in PLIN2$^{-/-}$ and**
352 **CPT2$^{-/-}$ macrophages**
353 We also analyzed transcriptomes from intracellular *Mtb* from scrambled controls, FATP1$^{-/-}$, CPT2^{-}
354 $^{/-}$ and PLIN2$^{-/-}$ macrophages in parallel with host transcriptomes in Fig. 5A. Using an adjusted p-
355 value of < 0.1 and an absolute log2 fold change > 1.4, 0 genes were DE in FATP1$^{-/-}$ macrophages,
356 105 *Mtb* genes were DE in PLIN2$^{-/-}$ macrophages (69 up, 36 down) and 10 genes were DE in CPT2^{-}
357 $^{/-}$ macrophages (3 up, 7 down) (Fig. 6A). Despite being restrictive to *Mtb* growth (Fig. 1C) and
358 appearing more pro-inflammatory (Fig. 5D), FATP1$^{-/-}$ macrophages did not elicit a detectable shift
359 in the transcriptional response in *Mtb,* compared to control host cells. We speculate that pro-
360 inflammatory responses in FATP1$^{-/-}$ macrophages could be enough to restrict the growth of
361 bacteria, but the resulting compensatory responses as evidenced by the upregulation of
362 macrophage scavenger receptors (Fig. S7A) alleviate some of the stresses that a lack of fatty acid
363 import could be duly exerting on the bacteria. PLIN2$^{-/-}$ macrophages appeared to elicit the
364 strongest transcriptional response from *Mtb* which is consistent with our CFU data (Fig. 1C) as
365 PLIN2$^{-/-}$ macrophages exhibited the strongest growth restriction. Among the DE genes in *Mtb*
366 from PLIN2$^{-/-}$ macrophages, a significant number of upregulated genes are involved in nutrient
367 assimilation (Fig. 6B). *Mtb* in PLIN2$^{-/-}$ macrophages upregulated CobU (Rv0254c) which is
368 predicted to be involved in the bacteria's cobalamin (Vitamin B_{12}) biosynthesis. Vitamin B_{12} is an
369 important cofactor for the activity of *Mtb* genes required for cholesterol and fatty acid utilization
370 (45, 51). Genes involved in de novo long chain fatty acid synthesis (AccE5, Rv281) (52), cholesterol
371 breakdown (HsaD, Rv3569c) (53), β-oxidation of fatty acids (EchA18, Rv3373; FadE22, Rv3061c)
372 (54), purine salvage (Apt, Rv2584c) (55) and tryptophan metabolism (56) were also upregulated
373 in *Mtb* from PLIN2$^{-/-}$ macrophages (Fig. 6B). This metabolic re-alignment response is seen most
374 frequently under nutrient limiting conditions (11, 12, 57). *Mtb* in PLIN2$^{-/-}$ macrophages also
375 appears to experience a significant level of other cellular stresses as genes involved in DNA
376 synthesis and repair, general response to oxidative stress and PH survival in the phagosome

377 (DnaN, Rv0002; RecF, Rv0003; DinF, Rv2836c; Rv3242c, Rv1264) were upregulated (Fig. 6B).
378 Amongst the down-regulated genes in *Mtb* in PLIN2$^{-/-}$ macrophages, FurA (Rv1909c), a KatG
379 repressor was the most significant (Fig. 6B, Table. S4). FurA downregulation derepresses the
380 catalase peroxidase, KatG, which promotes *Mtb* survival in oxidative stress conditions (58). These
381 data suggest that PLIN2$^{-/-}$ macrophages could be, in part, restricting *Mtb* growth by increasing
382 production of ROS. The data also suggest that, contrary to a previous report (23), blocking lipid
383 droplet formation in host macrophages does place increased nutritional and oxidative stress on
384 intracellular *Mtb*.

385 CPT2$^{-/-}$ macrophages elicited a modest shift in transcriptional response from *Mtb*, and the
386 majority of the DE genes (8 out of 10) were also DE in PLIN2$^{-/-}$ macrophages (Table. S4). This in in
387 agreement with the host transcription response as CPT2$^{-/-}$ and PLIN2$^{-/-}$ macrophages share similar
388 candidate anti-bacterial responses (Fig.5A-C, S5). In common with the *Mtb* transcriptome
389 response in PLIN2$^{-/-}$ macrophages, upregulated genes in *Mtb* isolated from CPT2$^{-/-}$ macrophages
390 included those involved in response to oxidative stress (DinF, Rv2836c) (Table. S4). To substantiate
391 some of these pathways, we assessed the levels of total cellular ROS in FATP1$^{-/-}$, PLIN2$^{-/-}$ and CPT2^{-}
392 $^{/-}$ macrophages in both *Mtb* infected and uninfected conditions by staining the cells with the
393 Invitrogen CellROX dye and confocal microscopy analysis of live stained cells. In both infected and
394 uninfected conditions, all the 3 mutants displayed significantly elevated total cellular ROS when
395 compared to scramble controls (Fig. S9A, S9B).
396

397 **Inhibitors of lipid metabolism block intracellular growth of *Mtb* in macrophages but not in broth**
398 **culture**

399 We next examined if pharmacological inhibitors would phenocopy the growth inhibition
400 phenotypes we observed with specific gene deletions. Compounds which modulate lipid
401 homeostasis are currently being investigated for HDT against TB, which is an area of considerable
402 interest (59). Such compounds include metformin, a widely used anti-diabetic drug which
403 activates AMPK, inhibits fatty acid synthesis and promotes β-oxidation of fatty acids (21, 60).
404 Chemical inhibition of fatty acid β-oxidation is already known to promote macrophage control of
405 *Mtb* (11, 25). We targeted macrophage lipid homeostasis with trimetazidine (TMZ), an inhibitor

406 of β-oxidation of fatty acids, metformin, and an FATP1 inhibitor, FATP1 In (61). We assessed the
407 impact of these compounds on extracellular *Mtb* cultured in broth over 9 days in the presence of
408 the inhibitors (DMSO, TMZ; 500 nM, Metformin; 2 mM, FATP1 In; 10 μM, Rifampicin; 0.5 μg/ml).
409 None of the 3 lipid metabolism inhibitors had a measurable effect on *Mtb* growth in liquid culture
410 media when compared to DMSO controls (Fig. 7A). Treatment with rifampicin completely blocked
411 bacterial growth under the same conditions (Fig. 7A). We next infected scrambled sgRNA control
412 macrophages with *Mtb* at MOI 0.5. Inhibitors were added to infected macrophages 3 hours post
413 infection and bacterial CFUs were enumerated 4 days post treatment. Consistent with previous
414 observations (21, 25), TMZ and metformin significantly reduced bacterial loads in macrophages
415 when compared to DMSO controls (Fig.7B). Similarly, FATP1 In also impacted the intracellular
416 growth of *Mtb* (Fig. 7B). The results provide independent data that both genetic and chemical
417 modulation of fatty acid metabolism at different steps in the process negatively impacts
418 intracellular growth of *Mtb*.
419
420 **Discussion**
421 It is clearly established that host derived fatty acids and cholesterol are important carbon sources
422 for *Mtb* (22). However, the relationship between *Mtb* and the infected host cell lipid metabolism
423 remains a subject of conjecture. In this report, we characterized the role of macrophage lipid
424 metabolism on the intracellular growth of *Mtb* by a targeted CRISPR mediated knockout of host
425 genes involved in fatty acid import, sequestration and catabolism. Macrophage fatty acid uptake
426 is mediated by the scavenger receptor CD36 and specialized long chain fatty acid transporters,
427 FATP1 and FATP4 (62). Earlier studies reported that a deficiency of CD36 enhances macrophage
428 control of *Mtb,* albeit to a modest degree (27). Work from Hawkes et al.(27) indicated that the
429 anti-microbial effectors in CD36 deficient macrophages were not due to bacterial uptake
430 deficiencies, differences in the rate of *Mtb* induced host cell death, production of ROS or pro-
431 inflammatory cytokines (27). We similarly observed a moderate *Mtb* growth restriction
432 phenotype in our CRISPR generated $CD36^{-/-}$ macrophages. However, a strong growth restriction
433 of *Mtb* was observed when we knocked out the long chain fatty acid transporter, FATP1. $FATP1^{-/-}$
434 macrophages displayed altered metabolism characterized by stabilization of HIF-1α, activated

435 AMPK, increased glycolysis and reduced mitochondrial functions. Given that both CD36 and
436 FATP1 perform similar functions, it is expected that they should be some degree of compensation
437 between the transporters when either of the genes are deleted. Indeed, we found out that FATP1
438 knockout resulted in the upregulation of other lipid import transporters (MSR1, ABCC1). This
439 would be consistent with the moderate anti-*Mtb* phenotypes in CD36$^{-/-}$ macrophages which could
440 easily be compensated by the presence of FATPs to alleviate the reduction in fatty acid supply
441 experienced by intracellular *Mtb*. However, the FATP1$^{-/-}$ macrophage phenotype appears to be
442 more severe on *Mtb* and could be exacerbated by an elevated pro-inflammatory response as has
443 been reported previously both *in vitro* and *in vivo* (33).
444
445 After uptake into the cells, most fatty acids either undergo β-oxidation in the mitochondria to
446 provide energy or are esterified with glycerol phosphate to form triacylglycerols that may be
447 incorporated into lipid droplets in the endoplasmic reticulum (62). Over the last 2 decades, it has
448 been believed that lipid droplets are a nutrient source for *Mtb* in macrophages (4-7). However,
449 recent work indicates lipid droplets may serve as centers for the production of pro-inflammatory
450 markers and anti-microbial peptides (23, 24). It has also been reported that bone marrow
451 macrophages derived from PLIN2$^{-/-}$ mice did not have defects in the formation of lipid droplets
452 and supported robust intracellular *Mtb* replication (23). However, our mutant macrophages with
453 myeloid specific knockout of PLIN2 are unable to form lipid droplets and are defective in
454 supporting the growth of *Mtb*. The discrepancies with previous observations (23) could be a
455 consequence of compensatory responses to PLIN2 knockout in whole mice which when
456 performed at embryonic level would allow for sufficient time for the cells to recover by
457 upregulating related PLIN isoforms. In fact, PLIN2$^{-/-}$ macrophages displayed the strongest anti-
458 *Mtb* phenotypes amongst our mutants exhibiting activated AMPK, increased glycolysis and
459 autophagy and impaired mitochondrial functions. *Mtb* isolated from PLIN2$^{-/-}$ macrophages
460 displayed signatures of severe nutrient limitation and oxidative stress damage.
461 It has also been previously reported that chemical, genetic or miR33 mediated blockade
462 of fatty acid β-oxidation in macrophages induces lipid droplet formation (19, 25) but that this
463 enhanced lipid droplet formation does not correlate with improved intracellular *Mtb* growth (25).

464 We observed a similar phenotype as CPT2$^{-/-}$ macrophages that generated larger and more
465 abundant lipid droplets than scrambled control macrophages were still restrictive to *Mtb* growth.
466 This implies that the presence or absence of lipid droplets does not in itself indicate whether a
467 macrophage will support or restrict *Mtb* growth, and that the anti-microbial environment extends
468 beyond simple nutrient availability.
469
470 In summary, our study shows that blocking macrophage's ability to import, sequester or
471 catabolize fatty acids chemically or by genetic knockdown impairs *Mtb* intracellular growth. There
472 are shared features between potential anti-microbial effectors in macrophages which lack the
473 ability to import (FATP$^{-/-}$) or metabolize fatty acids (PLIN2$^{-/-}$, CPT2$^{-/-}$) such as increased glycolysis,
474 stabilized HIF-1α, activated AMPK, enhanced autophagy and production of ROS. However, there
475 are also intriguing points of divergence as FATP$^{-/-}$ macrophages are more pro-inflammatory while
476 PLIN2$^{-/-}$ macrophages appear to be broadly anti-inflammatory. The routes to *Mtb* growth
477 restriction in these mutant macrophages are clearly more complex than the bacteria's inability to
478 acquire nutrients. The data further emphasizes that targeting fatty acid homeostasis in
479 macrophages at different steps in the process (uptake, storage and catabolism) is worthy of
480 exploring in the development of new therapeutics against tuberculosis.
481
482
483
484
485
486
487
488
489
490
491
492

493 **Materials and methods**

494 All materials and methods are as described (47) unless otherwise specified.

495

496 **Flow cytometry and western blot analysis**

497 Generation of CRISPR mutant Hoxb8 macrophages was carried out described previously (47).
498 Antibodies used for both western blot and flow cytometry were as follows: rat anti-Mouse
499 CD36:Alexa Fluor®647 (Biorad, 10 µl/million cells), rabbit anti-PLIN2 (Proteintech, 1:1000), rabbit
500 anti-FATP1 (Affinity biosciences, 1:1000), rabbit anti-CPT1A antibody (Proteintech, 1:1000), rabbit
501 anti-CPT2 antibody (Proteintech, 1:1000), rabbit anti-HIF-1α antibody (Proteintech, 1:1000),
502 rabbit anti-AMPKα(1:1000, Cell signalling Technology), rabbit anti-Phospho-AMPKα(1:500, Cell
503 signalling Technology), rabbit anti-LC3B (1:1000, Cell signalling Technology) and rabbit anti-β Actin
504 (1:1000, Cell Signalling Technology). For western blots, secondary antibodies used were anti-
505 rabbit/mouse StarBright Blue 700 (1:2500, Biorad). Blots were developed and imaged as
506 described previously (47).

507

508 **Staining for cellular lipid droplets**

509 Macrophages monolayers in Ibidi eight-well chambers were supplemented with exogenous 400
510 µM oleate for 24 hours to induce the formation of lipid droplets (32). Cells were then fixed in 4%
511 paraformaldehyde and stained with BODIPY™ 493/503 (Invitrogen, 1 µg/ml) in 150 mM sodium
512 chloride. Stained cells were mounted with media containing DAPI and imaged using a Leica SP5
513 confocal microscope.

514

515 **Seahorse XF palmitate oxidation stress test**

516 A modified Seahorse mitochondrial stress test was used to measure macrophage's ability to
517 oxidize palmitate in substrate limiting conditions. 2 days before the assay, 1 x 10^5 cells were plated
518 in Seahorse cell culture mini plates. 1 day before the assay, macrophage media was replaced with
519 the Seahorse substrate limited growth media (DMEM without pyruvate supplemented with 0.5
520 mM glucose, 1 mM glutamine, 1% FBS and 0.5 mM L-Carnitine). On the day of the assay, substrate
521 limited media was replaced with assay media (DMEM without pyruvate supplemented with 2 mM

522 glucose and 0.5 mM L-Carnitine). In selected treatment conditions, cells were either supplied with
523 bovine serum albumin (BSA), BSA palmitate or BSA palmitate plus etomoxir (4 µM). Oxygen
524 consumption rates (OCRs) were measured using the Mito Stress Test assay conditions as
525 described previously (47).
526
527 **Rescue of the *Mtb* ∆icl1 mutant in oleate supplemented media**
528 The *Mtb* H37Rv ∆*icl1* mutant expressing mCherry (46) was used for the rescue experiments. The
529 strain was maintained in 7H9 OADC broth as previously described (47) in the presence of
530 Kanamycin (25 µg/ml) and hygromycin (50 µg/ml). 24 hours before infection, macrophages were
531 cultured in normal macrophage media or media supplemented with 400 µM oleate. Cells were
532 then infected with the *Mtb* ∆*icl1* mutant at MOI 5. The bacterial mCherry signal was measured
533 on day 0 and day 5 post infection on an Envision plate reader (PerkinElmer). Oleate was
534 maintained throughout the experiment in the rescue assay conditions.
535
536 **Measurement of total cellular ROS**
537 Uninfected or *Mtb* infected macrophages monolayers in Ibidi eight-well chambers were stained
538 with the CellROX Deep Red dye (Invitrogen) as per manufacturer's staining protocol. Live stained
539 cells were imaged on a Leica SP5 confocal microscope. Z-stacks were re-constructed in ImageJ
540 from which mean fluorescence intensities (MFI) for individual cells were obtained.
541
542 **Datasets** The RNA-seq data from the Dual RNA-seq analysis of infected mouse macrophages,
543 which includes both macrophage and Mtb reads are available in GEO: GSE270571.
544
545 **Acknowledgements**
546 We would like to thank Dr. Jen K. Grenier and Ann E. Tate from the Cornell BRC Transcriptional
547 Regulation and Expression Facility for their help with the development of dual RNA-Seq protocols.
548 This work was supported by grants from the National Institutes of Health (AI155319, AI162598,
549 and OD032135), Bill and Melinda Gates Foundation and the Mueller Health Foundation to D.G.R.
550 EJ was supported by T32AI007349

551 **References**
552

553 1. WHO (2023) Global tuberculosis report 2023. World Health Organisation, Geneva,
554 Switzerland.

555 2. S. B. Cohen *et al.*, Alveolar Macrophages Provide an early *Mycobacterium tuberculosis*
556 niche and initiate dissemination. *Cell Host Microbe* **24**, 439-446.e434 (2018).

557 3. A. J. Wolf *et al.*, *Mycobacterium tuberculosis* infects dendritic cells with high frequency
558 and impairs their function in vivo. *J Immunol* **179**, 2509-2519 (2007).

559 4. P. Peyron *et al.*, Foamy macrophages from tuberculous patients' granulomas constitute a
560 nutrient-rich reservoir for *M. tuberculosis* persistence. *PLoS Pathog* **4**, e1000204 (2008).

561 5. D. G. Russell, P. J. Cardona, M. J. Kim, S. Allain, F. Altare, Foamy macrophages and the
562 progression of the human tuberculosis granuloma. *Nat Immunol* **10**, 943-948 (2009).

563 6. V. Singh *et al.*, *Mycobacterium tuberculosis*-driven targeted recalibration of macrophage
564 lipid homeostasis promotes the foamy phenotype. *Cell Host Microbe* **12**, 669-681 (2012).

565 7. J. Daniel, H. Maamar, C. Deb, T. D. Sirakova, P. E. Kolattukudy, Mycobacterium tuberculosis
566 uses host triacylglycerol to accumulate lipid droplets and acquires a dormancy-like
567 phenotype in lipid-loaded macrophages. *PLoS Pathog* **7**, e1002093 (2011).

568 8. E. J. Muñoz-Elías, J. D. McKinney, Mycobacterium tuberculosis isocitrate lyases 1 and 2 are
569 jointly required for in vivo growth and virulence. *Nat Med* **11**, 638-644 (2005).

570 9. A. K. Pandey, C. M. Sassetti, Mycobacterial persistence requires the utilization of host
571 cholesterol. *Proc Natl Acad Sci U S A* **105**, 4376-4380 (2008).

572 10. A. Brzostek, J. Pawelczyk, A. Rumijowska-Galewicz, B. Dziadek, J. Dziadek, Mycobacterium
573 tuberculosis is able to accumulate and utilize cholesterol. *J Bacteriol* **191**, 6584-6591
574 (2009).

575 11. L. Huang, E. V. Nazarova, S. Tan, Y. Liu, D. G. Russell, Growth of Mycobacterium tuberculosis
576 in vivo segregates with host macrophage metabolism and ontogeny. *J Exp Med* **215**, 1135-
577 1152 (2018).

578 12. D. Pisu, L. Huang, J. K. Grenier, D. G. Russell, Dual RNA-Seq of Mtb-Infected Macrophages
579 In Vivo Reveals Ontologically Distinct Host-Pathogen Interactions. *Cell Rep* **30**, 335-350
580 e334 (2020).

581 13. D. Pisu *et al.*, Single cell analysis of M. tuberculosis phenotype and macrophage lineages
582 in the infected lung. *J Exp Med* **218** (2021).

583 14. B. M. Cumming, K. W. Addicott, J. H. Adamson, A. J. Steyn, Mycobacterium tuberculosis
584 induces decelerated bioenergetic metabolism in human macrophages. *Elife* **7** (2018).

585 15. M. Podinovskaia, W. Lee, S. Caldwell, D. G. Russell, Infection of macrophages with
586 Mycobacterium tuberculosis induces global modifications to phagosomal function. *Cell*
587 *Microbiol* **15**, 843-859 (2013).

588 16. M. J. Kim *et al.*, Caseation of human tuberculosis granulomas correlates with elevated host
589 lipid metabolism. *EMBO Mol Med* **2**, 258-274 (2010).

590 17. Y. S. Kim *et al.*, PPAR-α Activation Mediates Innate Host Defense through Induction of TFEB
591 and Lipid Catabolism. *J Immunol* **198**, 3283-3295 (2017).

592 18. P. E. Almeida *et al.*, Mycobacterium bovis bacillus Calmette-Guérin infection induces TLR2-
593 dependent peroxisome proliferator-activated receptor gamma expression and activation:
594 functions in inflammation, lipid metabolism, and pathogenesis. *J Immunol* **183**, 1337-1345
595 (2009).

596 19. M. Ouimet *et al.*, Mycobacterium tuberculosis induces the miR-33 locus to reprogram
597 autophagy and host lipid metabolism. *Nat Immunol* **17**, 677-686 (2016).

598 20. S. P. Parihar *et al.*, Statin therapy reduces the mycobacterium tuberculosis burden in
599 human macrophages and in mice by enhancing autophagy and phagosome maturation. *J*
600 *Infect Dis* **209**, 754-763 (2014).

601 21. A. Singhal *et al.*, Metformin as adjunct antituberculosis therapy. *Sci Transl Med* **6**,
602 263ra159 (2014).

603 22. K. M. Wilburn, R. A. Fieweger, B. C. VanderVen, Cholesterol and fatty acids grease the
604 wheels of Mycobacterium tuberculosis pathogenesis. *Pathog Dis* **76** (2018).

605 23. M. Knight, J. Braverman, K. Asfaha, K. Gronert, S. Stanley, Lipid droplet formation in
606 Mycobacterium tuberculosis infected macrophages requires IFN-γ/HIF-1α signaling and
607 supports host defense. *PLoS Pathog* **14**, e1006874 (2018).

608 24. M. Bosch *et al.*, Mammalian lipid droplets are innate immune hubs integrating cell
609 metabolism and host defense. *Science* **370** (2020).

610 25. P. Chandra *et al.*, Inhibition of fatty acid oxidation promotes pacrophage control of
611 *Mycobacterium tuberculosis*. *mBio* **11**, e01139-20 (2020).

612 26. M. C. Kiritsy *et al.*, Mitochondrial respiration contributes to the interferon gamma
613 response in antigen-presenting cells. *Elife* **10**, e65109 (2021).

614 27. M. Hawkes *et al.*, CD36 deficiency attenuates experimental *Mycobacterial* infection. *BMC*
615 *Infect Dis* **10**, 299 (2010).

616 28. K. Nishiyama *et al.*, Fatty acid transport protein 1 enhances the macrophage inflammatory
617 response by coupling with ceramide and c-Jun N-terminal kinase signaling. *Intl*
618 *Immunopharmacol* **55**, 205-215 (2018).

619 29. A. Paul, B. H. Chang, L. Li, V. K. Yechoor, L. Chan, Deficiency of adipose differentiation-
620 related protein impairs foam cell formation and protects against atherosclerosis. *Circ Res*
621 **102**, 1492-1501 (2008).

622 30. G. Larigauderie *et al.*, Adipophilin enhances lipid accumulation and prevents lipid efflux
623 from THP-1 macrophages: potential role in atherogenesis. *Arterioscler Thromb Vasc Biol*
624 **24**, 504-510 (2004).

625 31. D. Conant *et al.*, Inference of CRISPR Edits from Sanger trace data. *CRISPR J* **5**, 123-130
626 (2022).

627 32. L. L. Listenberger, D. A. Brown, Fluorescent detection of lipid droplets and associated
628 proteins. *Curr Protoc Cell Biol* **Chapter 24**, Unit 24.22 (2007).

629 33. A. R. Johnson *et al.*, Metabolic reprogramming through fatty acid transport protein 1
630 (FATP1) regulates macrophage inflammatory potential and adipose inflammation. *Mol*
631 *Metab* **5**, 506-526 (2016).

632 34. L. E. Gleeson *et al.*, Cutting edge: *Mycobacterium tuberculosis* induces aerobic glycolysis
633 in human alveolar macrophages that is required for control of intracellular bacillary
634 replication. *J Immunol* **196**, 2444-2449 (2016).

635 35. L. Shi *et al.*, Infection with *Mycobacterium tuberculosis* induces the Warburg effect in
636 mouse lungs. *Sci Rep* **5**, 18176 (2015).

637 36. M. Belton *et al.*, Hypoxia and tissue destruction in pulmonary TB. *Thorax* **71**, 1145-1153
638 (2016).

639 37. R. Courtnay *et al.*, Cancer metabolism and the Warburg effect: the role of HIF-1 and PI3K.
640 *Mol Biol Rep* **42**, 841-851 (2015).

641 38. C. Li, J. Wang, J. F. Xu, J. Pi, B. Zheng, Roles of HIF-1α signaling in *Mycobacterium*
642 *tuberculosis* infection: new targets for anti-TB therapeutics? *Biochem Biophys Res*
643 *Commun* **711**, 149920 (2024).

644 39. D. Garcia, R. J. Shaw, AMPK: mechanisms of cellular energy sensing and restoration of
645 metabolic balance. *Mol Cell* **66**, 789-800 (2017).

646 40. M. G. Gutierrez *et al.*, Autophagy is a defense mechanism inhibiting BCG and
647 *Mycobacterium tuberculosis* survival in infected macrophages. *Cell* **119**, 753-766 (2004).

648 41. T. A. Gould, H. van de Langemheen, E. J. Muñoz-Elías, J. D. McKinney, J. C. Sacchettini, Dual
649 role of isocitrate lyase 1 in the glyoxylate and methylcitrate cycles in *Mycobacterium*
650 *tuberculosis. Mol Microbiol* **61**, 940-947 (2006).

651 42. J. D. McKinney *et al.*, Persistence of *Mycobacterium tuberculosis* in macrophages and mice
652 requires the glyoxylate shunt enzyme isocitrate lyase. *Nature* **406**, 735-738 (2000).

653 43. E. J. Muñoz-Elías, A. M. Upton, J. Cherian, J. D. McKinney, Role of the methylcitrate cycle
654 in *Mycobacterium tuberculosis* metabolism, intracellular growth, and virulence. *Mol*
655 *Microbiol* **60**, 1109-1122 (2006).

656 44. J. E. Griffin *et al.*, Cholesterol catabolism by *Mycobacterium tuberculosis* requires
657 transcriptional and metabolic adaptations. *Chem Biol* **19**, 218-227 (2012).

658 45. S. Savvi *et al.*, Functional characterization of a vitamin B12-dependent methylmalonyl
659 pathway in *Mycobacterium tuberculosis*: implications for propionate metabolism during
660 growth on fatty acids. *J Bacteriol* **190**, 3886-3895 (2008).

661 46. W. Lee, B. C. VanderVen, R. J. Fahey, D. G. Russell, Intracellular Mycobacterium
662 tuberculosis exploits host-derived fatty acids to limit metabolic stress. *J Biol Chem* **288**,
663 6788-6800 (2013).

664 47. N. V. Simwela *et al.*, Genome-wide screen of *Mycobacterium tuberculosis* infected
665 macrophages identified the GID/CTLH complex as a determinant of intracellular bacterial
666 growth. *bioRxiv* 10.1101/2024.05.06.592714, 2024.2005.2006.592714 (2024).

667 48. T. Wu *et al.*, clusterProfiler 4.0: a universal enrichment tool for interpreting omics data.
668 *Innovation (Camb)* **2**, 100141 (2021).

669 49. A. Vogel, J. S. Brunner, A. Hajto, O. Sharif, G. Schabbauer, lipid scavenging macrophages
670 and inflammation. *Biochim Biophys Acta Mol Cell Biol Lipids* **1867**, 159066 (2022).

671 50. R. J. Raggers, A. van Helvoort, R. Evers, G. van Meer, The human multidrug resistance
672 protein MRP1 translocates sphingolipid analogs across the plasma membrane. *J Cell Sci*
673 **112 (Pt 3)**, 415-422 (1999).

674 51. E. Campos-Pardos, S. Uranga, A. Picó, A. B. Gómez, J. Gonzalo-Asensio, Dependency on
675 host vitamin B12 has shaped *Mycobacterium tuberculosis* complex evolution. *Nat*
676 *Commun* **15**, 2161 (2024).

677 52. B. Bazet Lyonnet *et al.*, Pleiotropic effect of AccD5 and AccE5 depletion in acyl-coenzyme
678 A carboxylase activity and in lipid biosynthesis in *Mycobacteria*. *PLoS One* **9**, e99853
679 (2014).

680 53. N. A. Lack *et al.*, Characterization of a carbon-carbon hydrolase from *Mycobacterium*
681 *tuberculosis* involved in cholesterol metabolism. *J Biol Chem* **285**, 434-443 (2010).

682 54. D. Schnappinger *et al.*, Transcriptional adaptation of *Mycobacterium tuberculosis* within
683 macrophages: insights into the phagosomal environment. *J Exp Med* **198**, 693-704 (2003).

684 55. D. F. Warner, J. C. Evans, V. Mizrahi, Nucleotide Metabolism and DNA Replication.
685 *Microbiol Spectr* **2**, MGM2-0001-2013 (2014).

686 56. J. S. Lott, The tryptophan biosynthetic pathway is essential for *Mycobacterium*
687 *tuberculosis* to cause disease. *Biochem Soc Trans* **48**, 2029-2037 (2020).

688 57. M. E. Theriault *et al.*, Iron limitation in *M. tuberculosis* has broad impact on central carbon
689 metabolism. *Commun Biol* **5**, 685 (2022).

690 58. T. C. Zahrt, J. Song, J. Siple, V. Deretic, Mycobacterial FurA is a negative regulator of
691 catalase-peroxidase gene KatG. *Mol Microbiol* **39**, 1174-1185 (2001).

692 59. J. S. Kim, Y. R. Kim, C. S. Yang, Host-directed therapy in tuberculosis: targeting host
693 metabolism. *Front Immunol* **11**, 1790 (2020).

60. M. D. Fullerton *et al.*, Single phosphorylation sites in Acc1 and Acc2 regulate lipid homeostasis and the insulin-sensitizing effects of metformin. *Nat Med* **19**, 1649-1654 (2013).

61. T. Matsufuji *et al.*, Arylpiperazines as fatty acid transport protein 1 (FATP1) inhibitors with improved potency and pharmacokinetic properties. *Bioorg Med Chem Lett* **23**, 2560-2565 (2013).

62. L. Deng, S. Kersten, R. Stienstra, Triacylglycerol uptake and handling by macrophages: from fatty acids to lipoproteins. *Progress in Lipid Research* **92**, 101250 (2023).

722 **Figure legends**

723 **Fig.1 Knockdown of fatty acid import and metabolism genes restricts *Mtb* growth in**
724 **macrophages**. (A) Schematic of lipid import and metabolism genes in macrophages. Genes
725 targeted for CRISPR-Cas9 mediated knockdown are highlighted in red. (B-C) Scramble or indicated
726 mutant macrophages were infected with the *Mtb* Erdman strain at MOI 0.4. CFUs were plated 3
727 hours post infection (B) and on Day 5 (C) to determine intracellular *Mtb* replication rates. n=6;
728 ****, $P < 0.0001$.

729

730 **Fig. 2. *Mtb* infected macrophages with impaired fatty acid import and metabolism display**
731 **reduced mitochondrial activities and are more glycolytic**. (A) Seahorse flux analyses of scramble
732 or PLIN2$^{-/-}$, FATP1$^{-/-}$ and CPT2$^{-/-}$ macrophages infected with *Mtb* Erdman strain at MOI 1 24 hours
733 post infection. Oxygen consumption rates (OCR) were measured using the Cell Mito Stress Test
734 Kit (Agilent). Oligo, oligomycin; FCCP, fluoro-carbonyl cyanide phenylhydrazone; Rot/A, rotenone
735 and antimycin A. (B) Comparison of basal respiration and spare respiratory capacity (SRC) from A.
736 SRC was calculated by subtracting the normalized maximal OCR from basal OCR. n=3 (2 technical
737 repeats per replicate); ****, $P < 0.0001$. (C) Extracellular acidification rates (ECARs) of scramble
738 or PLIN2$^{-/-}$, FATP1$^{-/-}$ and CPT2$^{-/-}$ macrophages infected with *Mtb* as in A. ECARs were measured
739 using the Agilent Seahorse Glycolysis Stress Test kit. 2DG, 2-Deoxy-D-glucose. (D) Comparison of
740 basal glycolysis and spare glycolytic capacity (SGC) in the indicated mutant macrophages. SGC was
741 calculated as SRC above. n=3 (2 technical repeats per replicate); *, $P < 0.05$, ****, $P < 0.0001$.

742

743 **Fig. 3. Knockdown of fatty acid import and metabolism genes in macrophagesactivate AMPK**
744 **and stabilizes HIF-1α.** (A) Western blot analysis of HIF-1α in uninfected and *Mtb* infected
745 scramble or PLIN2$^{-/-}$, FATP1$^{-/-}$ and CPT2$^{-/-}$ macrophages. In *Mtb* infected conditions, cells were
746 infected with the bacteria at MOI 1 for 48 hours before preparation of cell lysates. (B) Western
747 blot analysis of total and phosphorylated AMPK in uninfected and *Mtb* infected scramble or
748 PLIN2$^{-/-}$, FATP1$^{-/-}$ and CPT2$^{-/-}$ *macrophages*. Cell lysates were prepared as in A.

749

750 **Fig. 4. Supplementation with exogenous oleate fails to rescue the *Mtb* Δicl1 mutant in PLIN2$^{-/-}$,**
751 **FATP1$^{-/-}$ and CPT2$^{-/-}$ macrophages**. (A) Scramble or indicated mutant macrophages were infected
752 with the *Mtb* H37Rv Δicl1 mutant expressing mCherry at MOI 5. Oleate supplementation (400
753 μM) was commenced 24 hours before infection in the treatment group, removed during *Mtb*
754 infection and re-added 3-hours post infection for the entire duration of the experiment. Growth
755 kinetics of *Mtb* were measured by monitoring mCherry fluorescence using a plate reader. n=4;
756 ****, $P < 0.0001$. (B) Uninfected scramble or FATP1$^{-/-}$ and CPT2$^{-/-}$ macrophages were
757 supplemented with 400 μM oleate for 24 hours. Cells were then fixed for 20 minutes and stained
758 for lipid droplet inclusions using the Bodipy 493/503 dye. DAPI was used as a counterstain to
759 detect nuclei.
760
761 **Fig. 5. Dual RNA sequencing to identify host and bacterial determinants of *Mtb* restriction in**
762 **macrophages with fatty acid import and metabolism knockdown genes**. (A) Principal
763 component analysis (PCA) of scramble or PLIN2$^{-/-}$, FATP1$^{-/-}$ and CPT2$^{-/-}$ macrophages
764 transcriptomes infected with the *Mtb* smyc'::mCherry strain at MOI 0.5 4 days post infection. (B)
765 Venn diagram of DE gene sets (Table S2) in PLIN2$^{-/-}$, FATP1$^{-/-}$ and CPT2$^{-/-}$ mutant macrophages as
766 compared to scramble showing overlapping genes. DE genes cutoff; abs ($\log_2$ fold change) > 0.3,
767 adjusted p-value < 0.05. (C-D) Tree plot of top 80 enriched gene ontology terms (biological
768 process) in *Mtb* infected PLIN2$^{-/-}$ and FATP1$^{-/-}$ upregulated genes.
769
770 **Fig. 6. Nutritional and oxidative stress define the core transcriptome response of *Mtb* inside**
771 **PLIN2$^{-/-}$ macrophages.** (A) Schematic showing DE genes in *Mtb* transcriptomes isolated from
772 PLIN2$^{-/-}$, FATP1$^{-/-}$ and CPT2$^{-/-}$ macrophages in Fig.5A. (B) Heatmaps of nutritional and oxidative
773 stress DE genes in PLIN2$^{-/-}$ macrophages. Arrows show genes which are also DE in CPT2$^{-/-}$
774 macrophages in a similar trend (Table S4).
775
776 **Fig. 7. Inhibitors of fatty acid transport and metabolism block intracellular growth of *Mtb* in**
777 **macrophages.** (A) Growth of *Mtb* in liquid broth in the absence of drug (DMSO) or presence of
778 metformin, FATP1 inhibitor (FATP1 In, 10 μM) and the β-oxidation of fatty acid inhibitor,

779 Trimetazidine (TMZ, 500 nM). *Mtb* Erdman was grown to log phase and diluted to OD_{600} 0.01 in
780 7H9 media in the presence of the above inhibitors. Growth kinetics were monitored by OD_{600}
781 measurements using a plate reader. Rifampicin (RIF) at 0.5 μg/ml was used as a total killing
782 control. (B) Scramble macrophages were infected with *Mtb* Erdman at MOI 0.5. Inhibitors were
783 added 3 hours post infection following which CFUs were plated 4 days post infection. n=5; **, P
784 < 0.01; ****, P < 0.0001.
785
786
787
788
789
790
791
792
793
794
795
796
797
798
799
800
801
802
803
804
805
806
807

808 **Figure 1.**

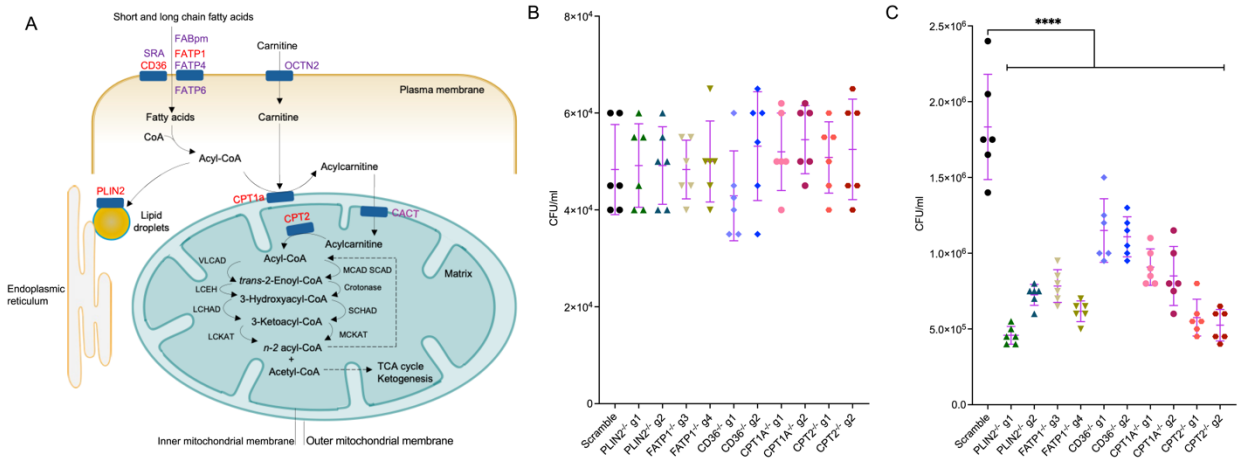

809

810

811 **Figure 2**

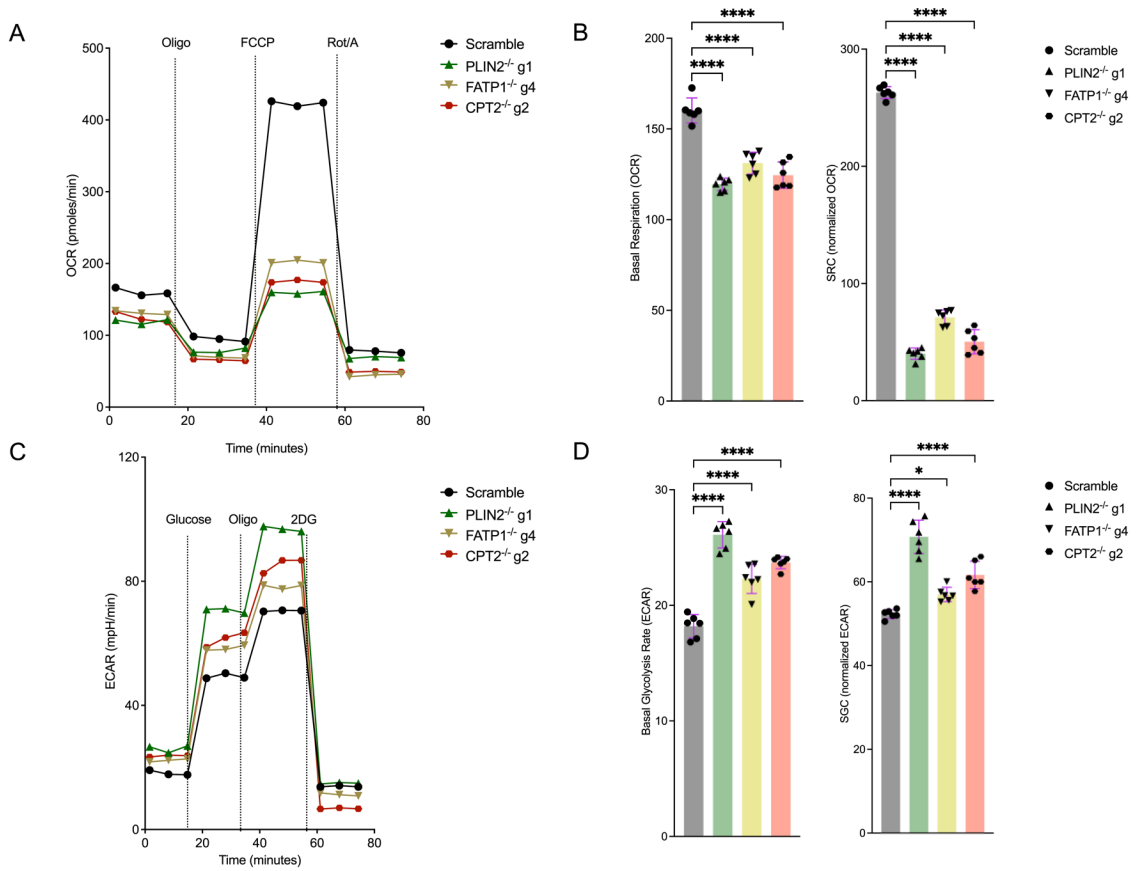

812

813

814 **Figure 3**

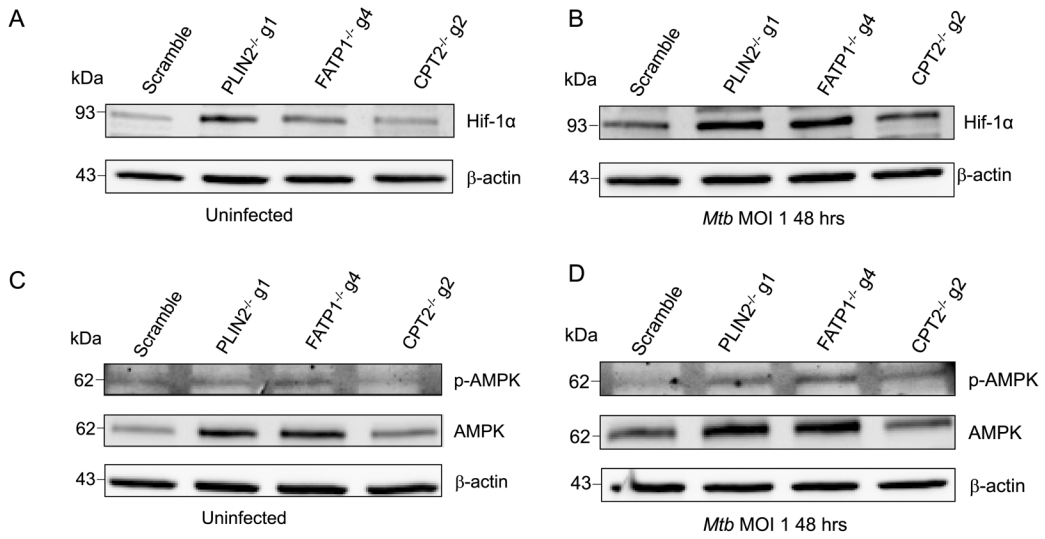

815

816

817 **Figure 4.**

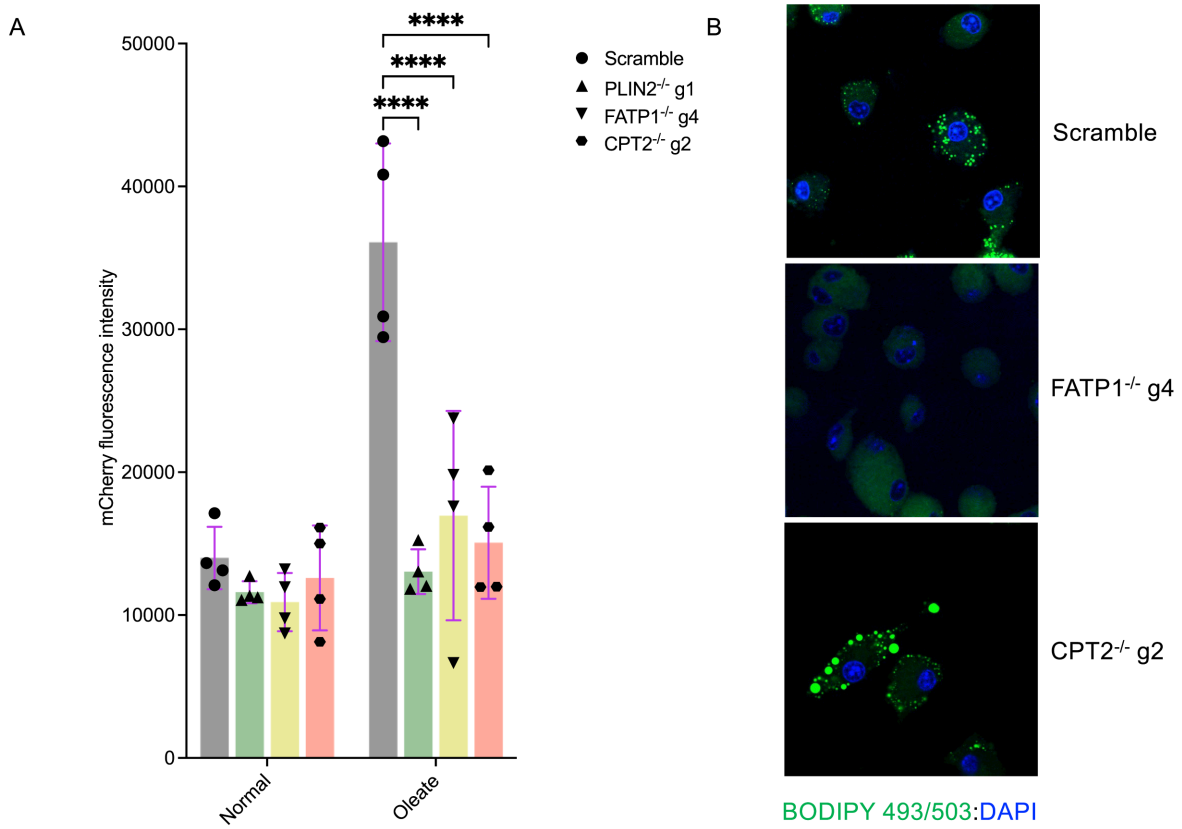

818

819

Figure 5.

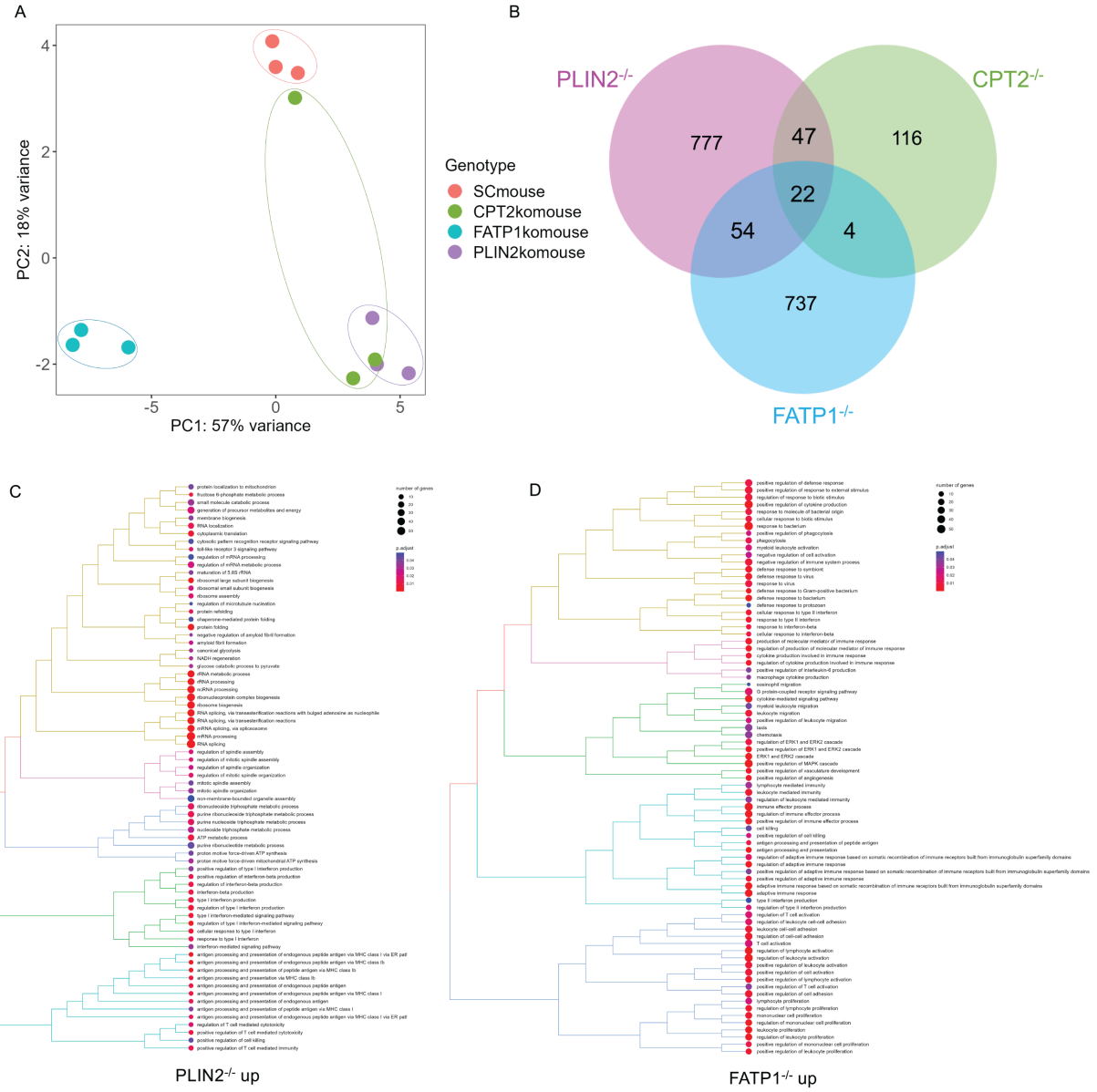
A
PC2: 18% variance
PC1: 57% variance
Genotype
SCmouse
CPT2komouse
FATP1komouse
PLIN2komouse
B
PLIN2-/-
CPT2-/-
FATP1-/-
777
47
116
22
54
4
737
C
D
PLIN2-/- up
FATP1-/- up

824 **Figure 6.**

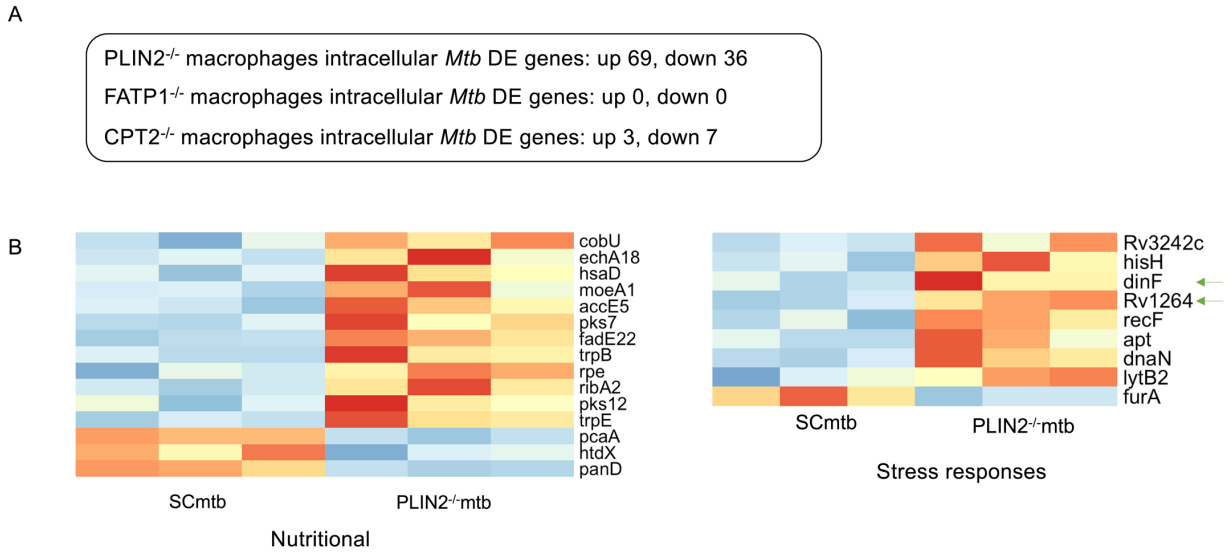

825

826 **Figure 7.**

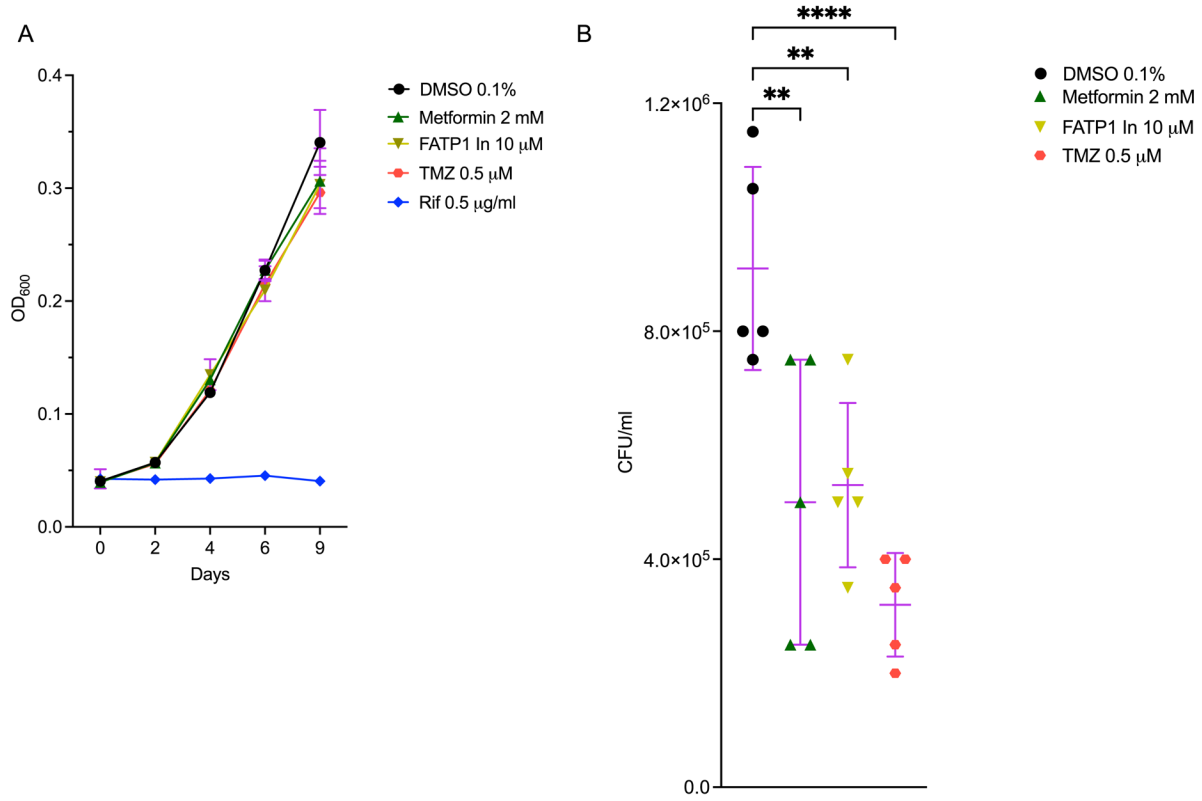

827

828